IEEE Access
Multidisciplinary | Rapid Review | Open Access Journal

Received August 15, 2020, accepted August 28, 2020, date of publication September 2, 2020, date of current version September 28, 2020.

Digital Object Identifier 10.1109/ACCESS.2020.3021104

Experimental Investigation of an Electro-Hydrostatic Actuator Based on the Novel Active Compensation Method

MINGKANG WANG[1,2], (Student Member, IEEE), YAN WANG[1,3], YONGLING FU[1,2], RONGRONG YANG[4], JIANG'AO ZHAO[1,2], AND JIAN FU[1,2], (Member, IEEE)

[1]Laboratory of Aerospace Servo Actuation and Transmission, Beihang University, Beijing 100191, China
[2]School of Mechanical Engineering and Automation, Beihang University, Beijing 100191, China
[3]School of Transportation Science and Engineering, Beihang University, Beijing 100191, China
[4]School of Mechanical and Electrical Engineering, Lanzhou University of Technology, Lanzhou 730050, China

Corresponding author: Jian Fu (fujian@buaa.edu.cn)

This work was supported in part by the Natural Science Foundation of China under Grant 61520106010, and in part by the Chinese Civil Aircraft Project under Grant MJ-2017-S49.

ABSTRACT For electro-hydrostatic actuators (EHAs), how to estimate and compensate for the combined effects of the severe nonlinearity caused by inner leakage and friction, the parametric uncertainties of the hydraulic components due to the environment and the external disturbance remain the primary issues. In this paper, a novel four-loop cascade control based on the active disturbance compensation method was proposed to address the abovementioned problem. First, by dividing the model of an EHA, two low-order estimators were obtained rather than a high-order estimator, which are easier to be implemented. Further, pressure information of two chambers of the EHA was applied in the proposed controller to compensate for the mismatching disturbances directly. Finally, the experimental results proved that the proposed method improved the robustness and static state error by approximately 35% and 33%, respectively.

INDEX TERMS EHA, servo control, ADCM, modeling, low velocity.

I. INTRODUCTION

The competition of Industry 4.0 has promoted the development of the industry all over the world. Therefore, machinery such as industrial robots, rehabilitation machines, and injection molding machines have been developed [1], [2]. In this mechanical equipment, hydraulic actuation systems are increasingly used because of the superiorities in power-to-weight ratio to traditional electric devices. However, hydraulic actuation systems pose many problems, such as limited installation space, difficulties in maintenance, and low efficiency. Thus, electro-hydrostatic actuators (EHAs) has been gaining increasing attention. Benefitting from the self-contained system, the external hydraulic oil source is not necessary for the EHA and thus, the EHA is much flexible than the HAS and much mature than EMA [3]. In addition, the adjustment of the piston's position can be achieved by regulating the rotating speed of a bi-direction brushless motor rather than using a servo valve, which results in significant reduction for the EHA in terms of the weight and the maintenance costs and an improvement in the efficiency [4], [5].

The velocity of the cylinder in an EHA depends mainly on the flow rate of the piston pump whose output links directly to the motor rotating speed [6]. However, when an EHA is applied in the situation where both slowness and steadiness are expected simultaneously, such as a flight motion simulator, problems remain because the unpredictable inner leakage of hydraulic components and static friction. On one hand, compared with the valve-controlled hydraulic actuator, the EHA is characterized as a lower dynamic system with a high nonlinearity especially at a low-velocity condition, namely dead zone. In this specific area, the combined effects of low efficiency of the pump and the unpredictable friction of the cylinder significantly impair the performance of the EHA. On the another hand, potential uncertainties on typical parameters, such as the bulk modulus and the leakage coefficient, introduce variables in ambient temperature, which brings external disturbance to the operating conditions [7], [8]. To tackle this problem, various control strategies are proposed to improve the performance of the EHA by attenuating the

The associate editor coordinating the review of this manuscript and approving it for publication was Mark Kok Yew Ng.

effects of the nonlinear friction, the leakage, and the parameter uncertainties.

A Proportional-Integral-Derivative (PID) controller is an effective control method in real applications because of its simplicity and fewer parameters. In [9], [10], and [11], fuzzy and adaptive PIDs were used to compensate for the disturbance but limited improvements were obtained for the EHA control. In addition, robust control have been used, especially the sliding mode control (SMC), which is a well-known robust control algorithm that can be used in both linear and nonlinear systems [12]–[22]. A discrete-time sliding mode control was conducted by Yang *et al.* [14] because of the high efficiency in compensating for the uncertainties in the EHA through an appropriate approach. It was observed that the discrete-time SMC effectively reduced the effects of uncertainties combined with a disturbance observer. Meanwhile, a cascade control formed by a combination of PID and SMC was proposed by Zhang and Qi [15], which was verified by numerical simulation. Wang *et al.* [17] analyzed the nonlinear friction characteristics of an EHA system and a nonlinear algorithm SMC implemented with partitioning and linearly quadratic optimization was developed to determine the sliding surface. However, improvements in SMC have not been able to avoid the chattering caused by switching. Therefore, Yang *et al.* [18] proposed a new reaching law to attenuate the chattering effect and a disturbance sliding mode observer (SMO) was applied to estimate the mismatching disturbance of the EHA. Robust control is an effective method to stabilize the EHA system and to deal with system uncertainties. However, it is too complicated to be applied in a real application, because it has features, such as extra coordinate transformation for mismatching disturbances and the design of a four-order SMO so that only simulation was completed.

Adaptive control, in particular for the model reference adaptive control (MRAC) [23], [24], was also introduced in the EHA. Guo *et al.* [25] proposed a saturated adaptive control to compensate for the anti-windup and the dynamic performance by using a Nussbaum function. To overcome the uncertainties, the disturbance observers were adopted combined with a passive-based model method and an adaptive backstepping control was also used to fit the uncertainties [26], [27]. A methodology for measuring the oil leakage directly by observing the differential between two encoders was designed by Sakaino and Tsuji [28] to construct a leakage compensator. A feedback modulator and a disturbance estimator were integrated to suppress the effects of the nonlinear static friction and the external disturbances, respectively. However, it is not suitable for an EHA because the motor connects to the pump directly.

Similar to the EHA, the friction in a hydraulic flight motion simulator affects its low velocity tracking capability. Thus, Yao *et al.* [29] proposed a self-adaptive control law in which the friction was divided into two parts, i.e. nominal slow-change friction and nonlinear fast-change friction, which were compensated by an adaptive law and a robust controller, respectively. However, adaptive control is an approach that is well-suited for controlling the internal leakage and friction rather than the external load. Further, parameter uncertainties are still unsolved. Then, a linear extended state observer (ESO) was introduced into an adaptive robust control by Wang *et al.* [30] to achieve an accurate estimation and compensation and a seven-order observer was subsequently proposed. Although the mathematical proof of the ESO has been provided, a gap between the theory and the practical application exists because the noise cannot be prevented, and the higher-order of the estimator is, the more sensitive to noise the estimator. Hence, an estimator whose order is more than three can be difficult to apply to a real application.

A novel ADCM-based cascade control inspired by the ESO [30], [31] combined with an adaptive approach was proposed in this paper. First, a nonlinear model of the EHA system is proposed. The effects of the oil leakage, nonlinear static friction, parameters perturbation, and volume efficiency of a piston pump were considered. The uncertainties were overcome with two approaches: nominal model-based compensation and estimator compensation through a nonlinear extended disturbance estimator (EDE). A four-loop cascade control based on an active disturbance compensation method (ADCM) implemented with a nonlinear control law was proposed to achieve significant attenuation in the noise influence. The contributions of this paper lie in the following areas:

1) The developed method provided a solution to high-order estimator, which is dispensable in the active compensation method by dividing a high-order EHA model into several low-order subsystems. Therefore, the order of ESO for each subsystem is lower than ESO for the total EHA system making it more suitable for the practical situation.

2) This method made full use of the measurable states of the EHA system. The application of pressure and pressure loop of the EHA in the controller provided a direct way to compensate for the mismatching disturbance. Hence, it is easier to be implemented than the conventional works.

3) Based on the simulation, the proposed method was successfully applied to an EHA position tracking system. The experimental results verified the performance by comparing with other methods.

The structure of this paper is demonstrated as follows. The modeling of the EHA and its modification are described in Section 2. Section 3 describes the development of the four-loop control. Then, an experimental validation process for the proposed algorithm is shown in Section 4. Section 5 draws the main conclusions and further work.

II. MODELING OF AN EHA SYSTEM

The EHA system is schematically shown in Fig. 1. The entire system is comprised of a symmetrical hydraulic cylinder, a bi-direction fixed displacement piston pump, and other subsidiary hydraulic components, including three check valves, two relief valves, two switching valves, a mode select valve, and an accumulator. The sensors for measuring position, pressure, the motor rotating speed, and motor current combined

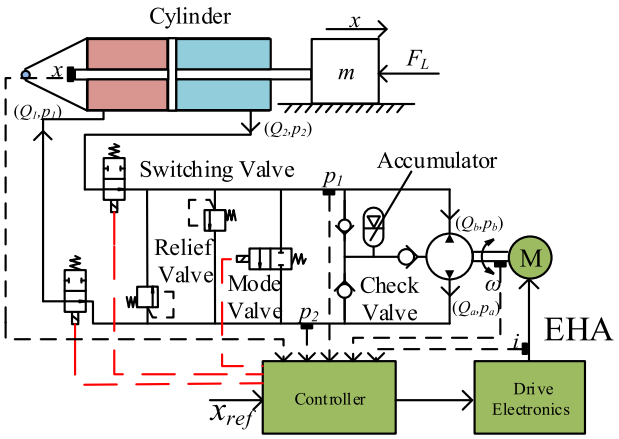

FIGURE 1. Schematic diagram of an EHA system.

with brushless DC motor (BLDCM) and power devices are also integrated. The operating principle of an EHA can be demonstrated as follows. Once the referenced position is received by the controller, the control signal for driving electronics is subsequently generated. The connection between the DC 270V wire and the BLDCM, which is governed by driving electronics, will switch itself at a significantly high frequency between on and off to achieve pulse-width modulation (PWM). By transforming electricity into rotation mechanical energy, the BLDCM drives the piston pump directly to complete the oil suction and discharge processes. The compression of oil results in the motion of the cylinder and in the linear motion of the load. Switching valves will be turned to the cut-off position, which stops the motion at the expected displacement. Similarly, the mode valve signal is used mainly for the maintenance situation.

The velocity of the cylinder depends mainly on the flow rate of the piston pump and the rotating speed of the BLDCM. The pressure of the rod chamber is also dominated by the combined effects of the external load and the internal friction.

A. MATHEMATICAL MODEL

If a Y-shaped BLDCM is used in an EHA, the three-phase winding voltages can be expressed as follows:

$$\begin{cases} u_a = L_a\dot{i}_a + Ri_a + e_a + U_N \\ u_b = L_b\dot{i}_b + Ri_b + e_b + U_N \\ u_c = L_c\dot{i}_c + Ri_c + e_c + U_N \end{cases}, \tag{1}$$

where e is the back Electro-Motive Force (EMF) and U_N is the central voltage of the three-phase windings. Generally, two-phase windings are in the conducting state and thus (1) can be rewritten as follows:

$$\begin{cases} u = L\dot{i} + Ri + K_e\omega \\ T_e = K_t i \\ J_{mp}\dot{\omega} = T_e - T_L - B_m\omega \end{cases}, \tag{2}$$

where u is the bus voltage and i is the bus current. L and R represent the line induction and line resistant, respectively. K_e means the back EMF coefficient while the electromagnetic torque T_e is proportional to the electromagnetic torque coefficient K_t. J_{mp} and B_m are the total inertia and total vicious friction coefficient of both the motor and the piston pump, respectively. T_L is the sum of the external load from the pump and the unmodeled friction.

Regarding the piston pump, the flow equation can be denoted as

$$\begin{cases} Q_a = \omega D_p - \varepsilon(p_a - p_b) - L_1(p_a - p_r) - \dfrac{V_a}{\beta_e}\dot{p}_a \\ Q_b = \omega D_p - \varepsilon(p_a - p_b) + L_1(p_b - p_r) + \dfrac{V_b}{\beta_e}\dot{p}_b \end{cases}, \tag{3}$$

where ε and L_1 are the inner and outer leakage coefficients of the pump, respectively, D_p is the pump displacement, p_a and p_b are the pressures of the two chambers of the piston pump, p_r is the system back pressure, and β_e represents the effective oil bulk modulus. Finally, Q_a and Q_b represent the inlet and outlet flow rates of the piston pump, respectively. The flow rate in two champers of the cylinder can be defined as follows:

$$\begin{cases} Q_1 = A\dot{x} + \frac{V_a}{\beta_e}\dfrac{dp_1}{dt} + L_2(p_1 - p_2) \\ Q_2 = A\dot{x} - \frac{V_b}{\beta_e}\dfrac{dp_2}{dt} - L_2(p_1 - p_2) \end{cases}, \tag{4}$$

where Q_1 and Q_2 are the supplied and returned flow rates of the cylinder, respectively. A indicates the effective ram area of the cylinder. V_a and V_b represent the initial volume of each chamber and L_2 is the internal leakage coefficient of the cylinder.

To further develop the EHA model shown in Fig. 1, some assumptions are made based on reality. First, the leakage of valves is much smaller than the inner leakage of the cylinder and the piston pump. Second, considering the short length of the flow channel in the manifold, the pressure drop resulted from linear loss of oil flowing is too small by comparing with the pressure drop caused by static friction of the cylinder and viscous friction of the piston pump. Hence, two rational assumptions are made:

Assumption 1: Flow rates consumed by all types of valves is quite low, which can be neglected.

Assumption 2: The length of the flow passage on the manifold is extremely short, hence, the pressure drop of oil is neglected.

Based on these assumptions combined with the flow rate continuity principle, for a double-rod symmetrical cylinder, the following equations can be obtained as follows:

$$Q_a = Q_1, Q_b = Q_2. \tag{5}$$

Considering the flow continuity and *Assumption* 2:

$$\dot{p}_a = \dot{p}_1, \dot{p}_b = \dot{p}_2, \dot{p}_1 = -\dot{p}_2. \tag{6}$$

Submitting (5) and (6) into (3) and (4), a simplified equation that denotes the relationship between the flow rate and the pressure change can be obtained:

$$D_p\omega = A\dot{x} + \frac{V_0}{\beta_e}\Delta\dot{p} + L_c\Delta p + Q_f, \tag{7}$$

where $V_0 = (V_a + V_b)/2$ is the volume of the system including chambers and pipes and $\Delta p = p_1$-p_2 is the pressure difference of the two chambers. L_c represents the total leakage coefficient of the system, consisting of the internal and external oil leakages. Q_f represents the unconsidered leakage.

The motion of the symmetrical piston can be described as follows:

$$A\Delta p = M\ddot{x} + B_c\dot{x} + K_s x + F_f + F_L, \tag{8}$$

where M indicates the sum of the mass of the piston, the rod, and the external workload. B_c means the viscous friction coefficient between the piston and its shell. K_s represents the elastic load (if it exists). F_f and F_L are the unmodeled friction of the cylinder and the external load force, respectively.

Finally, the state equations of the EHA system can be expressed as follows:

$$\begin{cases} \dot{x}_1 = x_2 \\ \dot{x}_2 = \dfrac{A}{M}x_3 - \dfrac{K_s}{M}x_1 - \dfrac{B_c}{M}x_2 - \dfrac{F_f + F_L}{M} \\ \dot{x}_3 = \dfrac{\beta_e}{V_0}D_p x_4 - \dfrac{A\beta_e}{V_0}x_2 - \dfrac{L_c\beta_e}{V_0}x_3 \\ \dot{x}_4 = \dfrac{1}{J_{mp}}(K_t x_5 - B_m x_4 - D_p x_3 - T_f) \\ \dot{x}_5 = \dfrac{1}{L}(u - Rx_5 - K_e x_4) \end{cases}, \tag{9}$$

where $x_i (i = 1,2\ldots5)$ are system state vectors that are defined as:

$$X = [x_1 x_2 x_3 x_4 x_5]^T = [x\dot{x}\,\Delta p\omega\, i]^T. \tag{10}$$

B. MODEL MODIFICATION

The aforementioned model is a purely mathematical model that omits typical factors, such as parametric uncertainty, and nonlinear factors that result from leakage and friction. However, in practical applications, these factors have to be considered. This paper focuses mainly on investigating the steadiness of an EHA, especially for the working condition at very low velocity. Therefore, a proposed model of the EHA system should be modified considering the nonlinear friction and time-varying leakage coefficient.

1) Nonlinear friction

Friction of the cylinder will affect its velocity, thus, a quadratic form of the friction that combines the characteristics of static friction, Coulomb friction and viscous friction can be written as follows[17]:

$$\begin{cases} F_{fn} = a_1\dot{x}^2 + a_2\dot{x} + a_3 (\dot{x} > 0) \\ F_{fn} = -a_1\dot{x}^2 + a_2\dot{x} - a_3 (\dot{x} < 0) \end{cases}, \tag{11}$$

where $a_i (i = 1,2,3)$ are the nonlinear friction coefficients.

2) Nonlinear leakage coefficient

According to the third equation in (9), the expression: $L_c = L_1 + L_2 + \varepsilon$ is unreasonable because L_2 is a nominal value whose true value is unattainable and is changing continuously with pressure difference between the two chambers of the cylinder. Nevertheless, it is acceptable to assume that $L_2(t)$ is a bounded function with a slow change. The values of L_1 and ε are also unobtainable, whereas the measurement for their overall effect is possible [32]. According to [32], the leakage of the pump is nearly invariable if the pressure difference between the inlet and outlet is constant. Because no dramatical changes occur on the pressure in different chambers when given a low cylinder velocity, the modified model of the pump can be denoted as follows:

$$D(\omega) = \begin{cases} D_p(1 - \left|\frac{\omega_0}{\omega}\right|), (|\omega| > |\omega_0|) \\ 0, (|\omega| \le |\omega_0|) \end{cases}, \tag{12}$$

where ω_0 is the threshold for the piston pump to compensate for the total leakage.

3) Other parameter perturbation

Generally, the effective ram area of the cylinder A, the overall mass M, and the volume of chambers V_0 can be measured precisely due to their insensitiveness to the changes in temperature and velocity. However, considering the viscous friction coefficient B_c and the effective oil bulk modulus β_e, only the nominal values are currently available. Therefore, for higher accuracy of the model, $(B_c + \Delta B_c)$ and $(\beta_e + \Delta\beta_e)$ are used in this paper, where ΔB_c and $\Delta\beta_e$ are also bounded values that represent the perturbations of B_c and β_e, respectively.

Therefore, combining the modification performed in all the considered parameters (i.e. a), b), c)) and (9), a modified nonlinear EHA model closer to the practical working condition yields:

$$\begin{cases} \dot{x}_1 = x_2 (a) \\ \dot{x}_2 = \dfrac{A}{M}x_3 - \dfrac{K_s}{M}x_1 - \dfrac{B_c + \Delta B_c}{M}x_2 - \dfrac{F_{fn} + F_L(t)}{M} (b) \\ \dot{x}_3 = \dfrac{\beta_e + \Delta\beta_e}{V_0}[D(\omega)x_4 - Ax_2 - L_2(t)x_3] (c) \\ \dot{x}_4 = \dfrac{1}{J_{mp}}(K_t x_5 - B_m x_4 - D_p x_3 - T_f) (d) \\ \dot{x}_5 = \dfrac{1}{L}(u - Rx_5 - K_e x_4) (e) \end{cases} \tag{13}$$

III. CONTROLLER DESIGN

According to (13), if x_d is set as a ramp signal, the anticipated value of $\dot{x}_1$, which is the true value of x_2 is expected to maintain a number with low magnitude. Likewise, the anticipated value of $\dot{x}_2$, which is the acceleration of the cylinder, will remain at zero. In other words, as stated in the second equation in (13), the system state x_3, which is also the pressure difference, is supposed to compensate for the external load disturbance $F_L(t)$, the nonlinear friction F_f, and the elastic load K_s (if exists). Additionally, the third equation denotes that the derivative of x_3 has dependence on the motor rotating speed x_4, the velocity of the cylinder x_2, a polynomial consisting of x_3 and the leakage coefficient, which is an unknown parameter. Thus, $\dot{x}_3$ remains zero only on the premise that the perturbations caused by parameter uncertainties, such as $\Delta\beta_e$ and $L_2(t)$, are compensated by the system state x_4. Therefore, a primary concern is how to determine properly and precisely the compensation to the parameter uncertainties.

According to (13), the dynamic characteristics of the machinery are indicated by the first two equations, while (13c) denotes the dynamic characteristics of the hydraulic subsystem where only the system pressure and flow rate are involved. Consequently, a cascade four-loop control algorithm based on the active disturbance compensation method (ADCM) is proposed. For a five-order EHA system, instead of a six-order extended disturbance estimator(EDE), two low-order estimators were applied in the proposed method, which is always preferred in practical application because no system is free from noise. The proposed method also makes full use of the measurable state of the EHA system by introducing a pressure loop. The method was able to compensate directly for mismatching disturbance without extra coordinating transformation.

A. ADCM FOR THE MECHANICAL SUBSYSTEM

If the mechanical subsystem is regarded as an independent system, its state equations can be written as follows:

$$\begin{cases} \dot{x}_1 = x_2 \\ \dot{x}_2 = G_p u_p + (-\dfrac{K_s}{M}x_1 - \dfrac{B_c + \Delta B_c}{M}x_2) + (-\dfrac{F_f}{M}) \\ \qquad\qquad +(-\dfrac{F_L(t)}{M}) \\ = G_p u_p + (-\dfrac{B_c}{M}x_2) + (-a_2 x_2) + h_p \\ y = x_1 \end{cases}, \tag{14}$$

where u_p represents the state x_3, which is the oil pressure difference and can be regarded as a virtual input. The system output is still the position of the cylinder. G_p is the ratio of the effective ram area of the cylinder A to the overall mass M, representing the sum of disturbances that act on the mechanical subsystem in the position loop. h_p can be considered as an ensemble item and the subscript p stands for parameters in the position loop. Accordingly, a double-integration subsystem can be obtained once the value of h_p and other variables are estimated and compensated accurately.

An extended disturbance estimator in which h_p is extended as a new state is expressed as follows:

$$\begin{cases} \dot{\hat{x}}_1 = \hat{x}_2 - l_{p1}(x_1 + n_p - \hat{x}_1) \\ \dot{\hat{x}}_2 = G_p x_3 + (-\frac{B_c}{M}\hat{x}_2) + (-a_2\hat{x}_2) \\ +\hat{h}_p - l_{p2} fal[(x_1 + n_p - \hat{x}_1), \alpha_{p1}, \delta] \\ \dot{\hat{h}}_p = -l_{p3} fal[(x_1 + n_p - \hat{x}_1), \alpha_{p2}, \delta] \end{cases}$$

$$fal[e, \alpha, \delta] = \begin{cases} \frac{e}{\delta^{1-\alpha}}, |e| \le \delta \\ |e|^{\alpha} sign(e), |e| > \delta \end{cases} \quad \delta{>}0, \tag{15}$$

where n_p is the measured noise at a specific position. $l_{pi}(i = 1,2,3)$ are Hurwitz. $\hat{x}_i$ and $\hat{h}_p$ represent the observed values of x_i and h_p, respectively. δ and α are tunable parameters of the EDE. Note that a detailed derivation of the stability of a nonlinear EDE is demonstrated in [33]. Therefore, the error dynamic equations of the observer can be obtained by subtracting (14) from (15):

$$\begin{cases} \dot{\tilde{x}}_1 = \tilde{x}_2 - l_{p1}(\tilde{x}_1 + n_p) \\ \dot{\tilde{x}}_2 = \tilde{h}_p - l_{p2} fal[(\tilde{x}_1 + n_p), \alpha_{p1}, \delta_p] \\ \dot{\tilde{h}}_p = \dot{h}_p - l_{p3} fal[(\tilde{x}_1 + n_p), \alpha_{p2}, \delta_p] \end{cases}, \tag{16}$$

where $\tilde{x}_1 = x_1 - \hat{x}_1, \tilde{x}_2 = x_2 - \hat{x}_2, \tilde{h}_p = h_p - \hat{h}_p$ are estimated error of x_1, x_2, h_p, respectively.

Applying a nonlinear control law in this situation, the output of the position loop is constructed as

$$\begin{aligned} x_3^* &= x_{3n} + x_{3c} \\ &= G_p^{-1}(k_{dp} fal(\dot{x}_d - \hat{x}_2, \alpha_{dp}, \delta_p) \\ &\quad + k_{pp} fal(x_d - \hat{x}_1, \alpha_{pp}, \delta_p)) \\ &\quad + G_p^{-1}(-\hat{h}_p + \frac{B_c}{M}\hat{x}_2 + a_2\hat{x}_2), \end{aligned} \tag{17}$$

where x_{3n} is a nominal control term and x_{3c} is a compensation term. Note that a detailed derivation of the stability of a nonlinear controller is introduced in [34].

Substituting (17) into (14), the dynamic error $e_p = x_1 - x_d$ can be expressed as follows:

$$\begin{aligned} &\ddot{e}_p + k_{dp}\dot{e}_p + k_{pp}e_p \\ &\quad = -k_{dp} fal(\tilde{x}_2, \alpha_{dp}, \delta_p) - k_{pp} fal(\tilde{x}_1, \alpha_{pp}, \delta_p) \\ &\qquad - \frac{B_c + a_2 M}{M}\tilde{x}_2 - \tilde{h}_p. \end{aligned} \tag{18}$$

$\tilde{x}_1, \tilde{x}_2$ and $\tilde{h}_p$ are bounded [33], [34] and therefore, according to Equation (15), the function $fal[e, \alpha, \delta]$ is bounded subsequently and the first polynomial in (18) will be bounded. In the same way, the second, third, and fourth are also bounded. As results, Equation (18) is bounded finally and the errors can be arbitrary small by tuning parameters.

B. ADCM IN THE HYDRAULIC SUBSYSTEM

The presence of the hydraulic subsystem has two aspects:

1) The effects of parameter perturbation, such as equivalent displacement $D(\omega)$, leakage coefficient L_2, and β_e, of the system cannot be neglected.

2) The pressure differences of a hydraulic system cannot be varied precisely because of the slight fluctuation induced by the external load, particularly for a situation where a cylinder is running at a very low velocity.

Hence, the state equations of the hydraulic subsystem can be expressed as

$$\begin{cases} \dot{x}_3 = \frac{\beta_e + \Delta\beta_e}{V_0} D(\omega) u_c - \frac{A(\beta_e + \Delta\beta_e)}{V_0} x_2 \\ -\frac{(L + \Delta L)(\beta_e + \Delta\beta_e)}{V_0} x_3 \\ = G_c u_c + \Delta G_c u_c - (\frac{A\beta_e}{V_0}x_2 + \frac{L\beta_e}{V_0}x_3) \\ -(\frac{A\Delta\beta_e}{V_0}x_2 + \frac{\Delta L\beta_e}{V_0}x_3 + \frac{L\Delta\beta_e}{V_0}x_3 + \frac{\Delta L\Delta\beta_e}{V_0}x_3) \\ = G_c u_c + (-\frac{A\beta_e}{V_0}x_2) + (-\frac{L\beta_e}{V_0}x_3) + h_c \\ y = x_3 \end{cases}, \tag{19}$$

where the virtual input u_c represents the state x_4, which is the rotating speed of the motor. The output $_y$ is the pressure difference of the hydraulic pump, h_c indicates the entity

disturbances affecting the oil subsystem, where the subscript c stands for parameters in the oil compression loop.

Then an EDE designed for the compression loop can be denoted as follows:

$$\begin{cases} \dot{\hat{x}}_3 = G_c x_4 + (-\frac{A\beta_e}{V_0}\hat{x}_2) + (-\frac{L\beta_e}{V_0}\hat{x}_3) \\ +\hat{h}_c - l_{c1}(\tilde{x}_3 + n_c) \\ \dot{\hat{h}}_c = -l_{c2} fal[(x_3 + n_c - \hat{x}_3), \alpha_{c1}, \delta_c] \end{cases} . \quad (20)$$

The output of the oil compression loop can be depicted as follows when a proportional control law is monotonously applied:

$$\begin{aligned} x_4^* &= x_{4n} + x_{4c} \\ &= G_c^{-1} k_{pc} fal(x_3^* - \hat{x}_3, \alpha_{pc}, \delta_c) \\ &\quad + G_c^{-1}(\frac{A\beta_e}{V_0}\hat{x}_2 + \frac{L\beta_e}{V_0}\hat{x}_3 - \hat{h}_c), \end{aligned} \quad (21)$$

where k_{pc} is the proportionality. Accordingly, the error dynamic equation of the compression loop can be written as

$$\begin{aligned} \dot{e}_c + k_{pc} e_c &= -\tilde{h}_c - k_{pc} fal(\tilde{x}_3, \alpha_{pc}, \delta_c) \\ &\quad - \frac{A\beta_e}{V_0}\tilde{x}_2 - \frac{L\beta_e}{V_0}\tilde{x}_3. \end{aligned} \quad (22)$$

The dual-PI control applied for the motor control is working in both speed and current loops and thus, the four-loop algorithm can be proposed as shown schematically in Fig. 2(a). The structures of the P-ADCM and the C-ADCM are illustrated by Figs. 2(b) and 2(c), respectively. As shown in Fig. 2(b), the position controller consists of nonlinear PD and EDE. The input of the position controller is reference and position feedback while its output is u_p. And u_p is exactly the reference of the compression controller shown in Fig. 2(c). Similarly, besides u_p, another input of compression controller is x_3. The output of compression controller, namely u_c(i.e., $\omega*$), is exactly the given instruction of dual-PI controller, which can be seen in Fig. 2(a).

According to error dynamic (22) can be rewritten as follows:

$$\begin{aligned} \dot{e}_c + k_{pc} e_c \le |H_c| + \frac{A\beta_e}{V_0}|X_2| \\ + \frac{L\beta_e}{V_0}|X_3| + k_{pc} fal(|X_3|, \alpha_{pc}, \delta_c). \end{aligned} \quad (23)$$

In this paper, h_c, x_2, x_3 represent external disturbances in the compression loop of the EHA, the speed of cylinder, and pressure, respectively. Therefore, because the states of C-EDE successfully converge around the real states, it is feasible that $\tilde{h}_c, \tilde{x}_2, \tilde{x}_3$ is bounded by $|H_c|, |X_2|, |X_3|$, respectively. k_{pc} is Hurwitz and thus, e_c,will converge to a limited range around zero in finite time t_c, and the velocity of convergence hinges on k_{pc}. Although the available range of k_{pc} is extended due to the adoption of a nonlinear function, a pretty large k_{pc} is still inadvisable because the priority of the stability of C-loop. Thus, at time t_c, we can obtain the following:

$$x_3 = x_3^* + e_c. \quad (24)$$

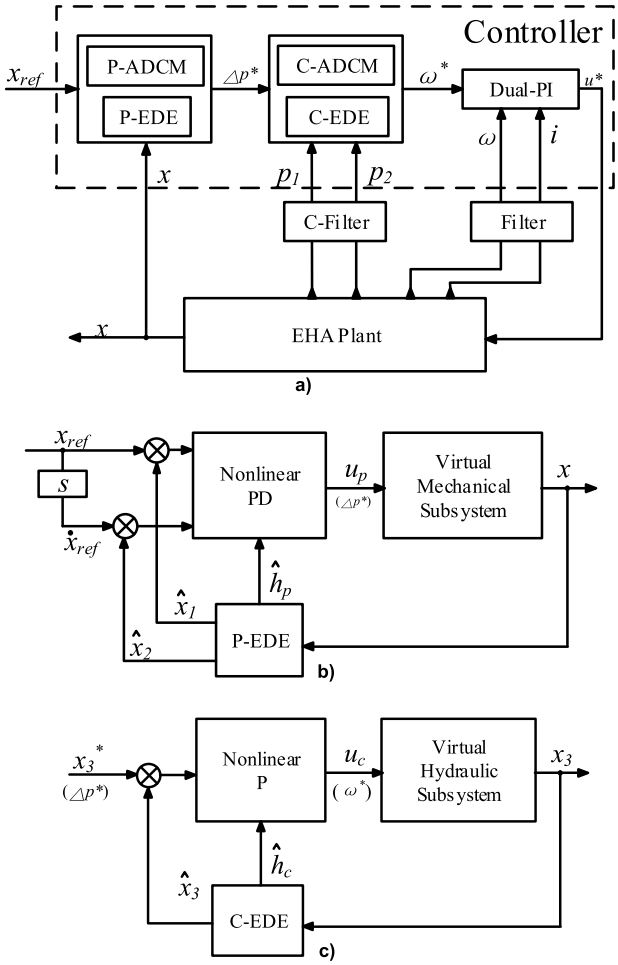

FIGURE 2. Schematic diagram of ADCM. a) Control block diagram of the EHA system. b) The control block diagram of the mechanical subsystem c) The control block diagram of the hydraulic subsystem.

Similarly, from (18),

$$\begin{aligned} \ddot{e}_p + k_{dp}\dot{e}_p + k_{pp} e_p \\ \le k_{dp} fal(|X_2|, \alpha_{dp}, \delta_p) + k_{pp} fal(|X_1|, \alpha_{pp}, \delta_p) \\ + \frac{B_c + a_2 M}{M}|X_2| + |H_p|, \end{aligned} \quad (25)$$

where $\tilde{h}_p, \tilde{x}_1$ are bounded by $|H_p|, |X_1|$, respectively and k_{pp}, k_{dp} are Hurwitz, which will ensure that the P-loop is stable. A finite converged time t_p can be obtained and e_p, the final position error, is also acquired at t_p.

$$x_1 = x_d + e_p \quad (26)$$

If $t_c \ll t_p$ can be guaranteed by tuning k_{pc}, k_{pp} and k_{dp}, according to the concept of the leading pole, the dynamic characteristic of the C-loop is too quick to impair the convergence of P-loop. Hence, the stability of the two subsystems is ensured.

IV. NUMERICAL AND EXPERIMENTAL VALIDATIONS

In this section, the proposed control method was validated using two approaches. First, a numerical simulation was

performed using the MATLAB/Simulink software package by tracking the sinusoidal, ramping, and square-wave signals; hence, both dynamic and static characteristics can be obtained. Similar studies were conducted on a PID controller and a developed adaptive PID (APID) for comparison. Then, an experimental study using a test rig was carried out in Section 4.2. A comparative study was also performed [35]–[37].

A. NUMERICAL SIMULATION

In the simulation study, the nonlinear model of the EHA built in Section 2 was used. Considering the uncertainties of friction and the leakage coefficients with a 50% deviation of the nominal value, some essential parameter setting is done as follows:

Friction dominating parameters: a_1 =21000, a_2 =-1450, a_3 =46.

Viscous friction coefficient: B_c =760N·s/m.

Effective bulk modulus of hydraulic oil: β_e =6.86 × 10^8Pa.

Cylinder leakage coefficient: L_2 =5 × 10^{-11}m^3/(s·Pa).

Simulation A: Low-speed validation

Two reference signals, sinusoidal signal and ramp signal, were selected to validate the low speed of the EHA. The former had a 5 mm amplitude and 0.05 Hz frequency, while the slope of the latter was defined as 0.1 mm/s. No external disturbance was applied in both situations. The curves of the considered signals are plotted in Figs. 3 and 4, respectively.

Simulation B: Dynamic performance validation

References were set to explore the dynamic response of the ADCM as follows:

x_{d1} =$sign$[1 × 10^{-2}sin(0.25πt)]+1 × 10^{-2}m, x_{d2} = 5 × 10^{-3}sin(πt)]m, and at t = 0s and when t = 4s, $x_{d2}$is arranged as x_{d2} = 5 × 10^{-3}sin(6πt)]m. Note that x_{d1} is a periodic step signal, while x_{d2} represents an intermediate and high-frequency simulation.

According to [38], the process of tuning parameters can be completed with desired bandwidth. And in this simulation parameters with the subscript "p" and "c" are set as follows:

$$\begin{cases} k_{pp} = 400, k_{dp} = 17 \\ \alpha_{pp} = \alpha_{p1} = 0.5 \\ \alpha_{dp} = \alpha_{p2} = 0.25 \\ \delta_p = 0.01 \\ l_{p1-3} = 100, 300, 1000 \end{cases} \text{and} \begin{cases} k_{pc} = 10, \\ \alpha_{pc} = \alpha_{c1} = 0.25 \\ \delta_c = 100 \\ l_{c1-2} = 5000, 15000 \end{cases}$$

Fig. 3(a) indicates that the proposed ADCM controller exhibited better dynamic performance than the two other counterparts i.e. the conventional PID and the APID, under the effects of the dead zone. The maximum position error of the PID and the APID controller were approximately 0.8mm and 0.55mm, respectively, which were higher than that of the proposed ADCM (0.3mm). In addition, the latter exhibited better transient performance and higher final tracking ability. An error bandwidth of around 0.4mm amplitude magnitude (shown as the red dotted lines in Fig. 3(b)) was used to evaluate the performance of the EHA system. The ADCM

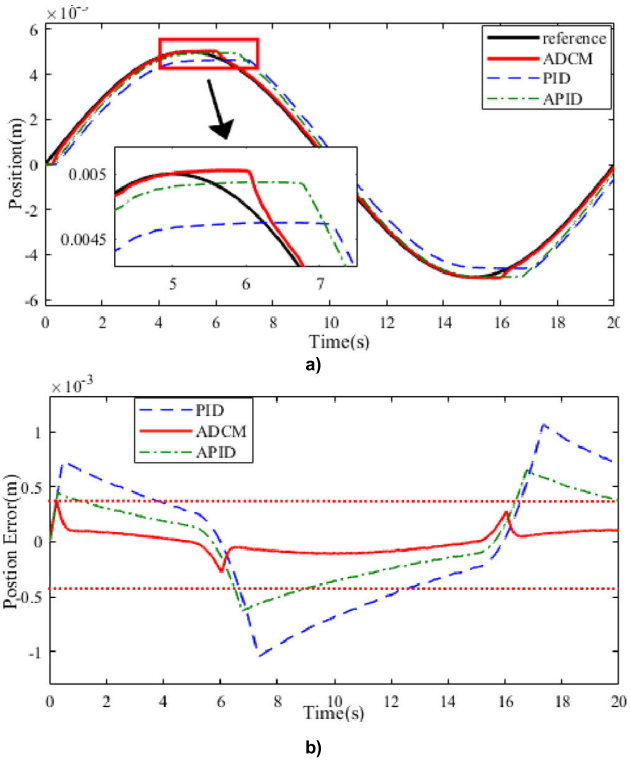

FIGURE 3. Sinusoidal signal tracking of the EHA model. a) Diagram of the position curves. b) Diagram of the position error.

was shown to be a satisfactory method for maintaining low velocity.

The comparison results of the ramp signal tracking by different methods are shown in Fig. 4, the nether diagram in Fig. 4(b) rescaled the middle part of the above diagram. The input of the EHA showed a slope of 0.1mm/s, which was somewhat small for an EHA with an effective movement of 110mm. Steps with 3mm were successively inputted to the position feedback as an external disturbance at the moment of 3s and 3.5s to simulate the bumped environment. Based on the zoomed parts in Fig. 4, it can be found that although the APID had improved ability for attenuating the effects of the dead zone, the result was still unsatisfactory for the low-velocity requirement. In contrast, the proposed ADCM showed superiority over its counterparts in tracking tiny signals, which was likely due to the nonlinear control law and the disturbance estimation and compensation provided by the EDE. However, the overshoot phenomenon found in the ADCM algorithm featured a 0.2mm excess presenting between 3s and 3.5s. This excess could possibly be a compromise result between the larger k_{pp} that contributed to the low-velocity tracking and the smaller k_{pp} hat was applied in following the step signals.

Fig. 5 plots the simulation results of the square-wave response obtained from different controllers. Meanwhile, Fig. 5(a) shows the ADCM exhibited better performance than either the APID or the PID in both the steady-state error and the speediness because of the less steady-state error and

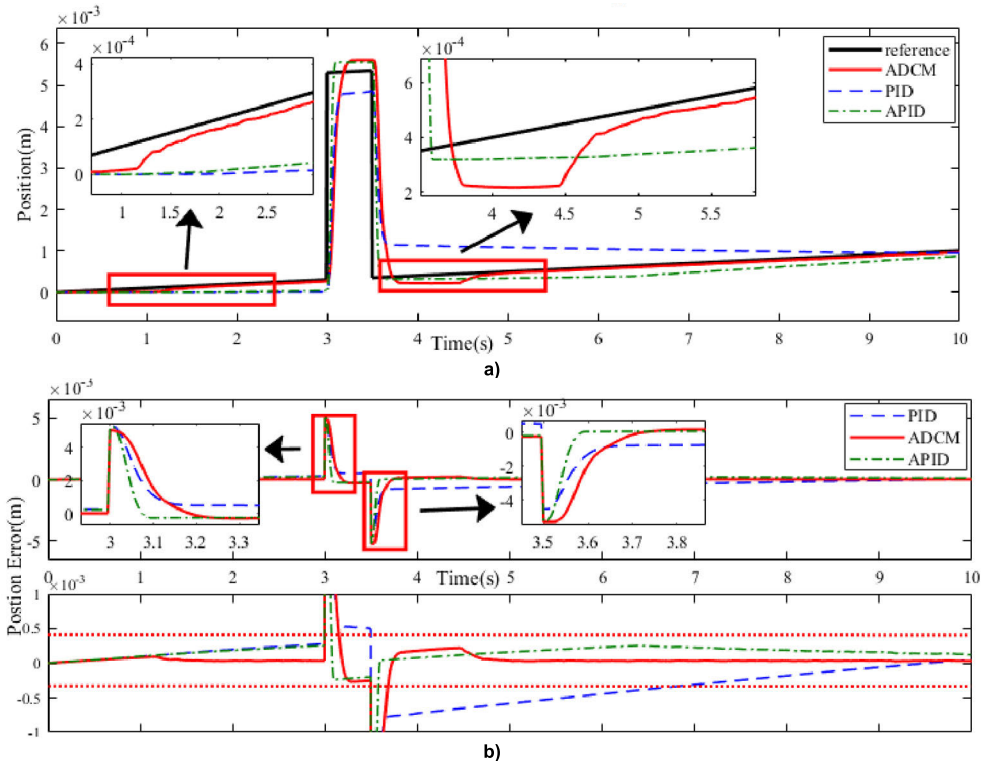

FIGURE 4. Ramping signal tracking of the EHA model. a) Diagram of the position curves. b) Diagram of the position error.

the better rapidness. In addition, as depicted in the zoomed parts in Fig. 5(b), the tracking error of the ADCM was below 0.1mm, which was much lower than that obtained by the APID (0.4 mm). Although no obvious overshoot was observed for the PID and the APID, the value for the ADCM was only around 3%, which is still acceptable. Additionally, it should be noted that an external load force FL=2000N suddenly appeared at 9s. This external disturbance was eliminated by the integral compensation in the APID, which however had features of time-consuming characteristics because of the unavoidable lagging of the integral effect. The green dot-dashed line and the blue dashed line indicated the limitations of the APID and the PID controllers based on deviation for a complex system, respectively. Using the pole-placement method, the latter was proven not well-suited for a system with unpredictable disturbance. Although the robustness can be somewhat improved for the APID because of its self-tuning proportional and integral parameters through an inherently upgraded law, the lagging caused by the integral effect was still difficult to prevent. On the contrary, the ADCM exhibited a rapid compensation ability to the external disturbance, which was found to significantly improve the robustness of the system, as indicated in the zoomed parts in Figs. 5(a) and (b). The transducer noise, i.e. the white noise with a bound magnitude of 0.5mm, was considered in the robustness assessment of the proposed ADCM.

Given that rapidness and accuracy are also assessment criteria for the EHA system, its dynamic characteristic was further explored in the following intermediate and high frequency tests by tracking a rapid-changing instruction, x_{d2}. The x_{d2} was defined as different frequency values that change with time evolution until 4s and no external workload was applied during this duration. Fig.6 reveals that the tracking performances of all the considered controllers were satisfactory in the medium band, although they all had flat-tops at both maximal and minimal positions, which resulted from the nonlinear friction of the cylinder combined with the dead zone of the pump. Differently, the proposed ADCM overcame the nonlinear zone with the contribution of the EDE.

The flat-top phenomenon was also found to be attenuated when the frequency of input rose to 3Hz, which indicated that the effect of the dead zone was indeed reduced by the high-frequency input. However, this reduction was accompanied by the phase lag and amplitude attenuation, as shown in the zoomed part in Fig. 6. Although no obvious attenuation was found in the cases of the ADCM and the APID, the trajectory phase for the latter was significantly deteriorated.

Based on the results shown in Fig. 7, it can be manifested that, even at the starting point, almost no error was found in the position estimation and the EDE achieved good estimation for the system state x_3 with an impulse impact. That results from no workload exists at the beginning so that the pressure differential between the two chambers is equal to zero which is also the initial condition of the estimator. Therefore, it is feasible to apply the estimated states in the ADCM and the compensation terms provided by the designed

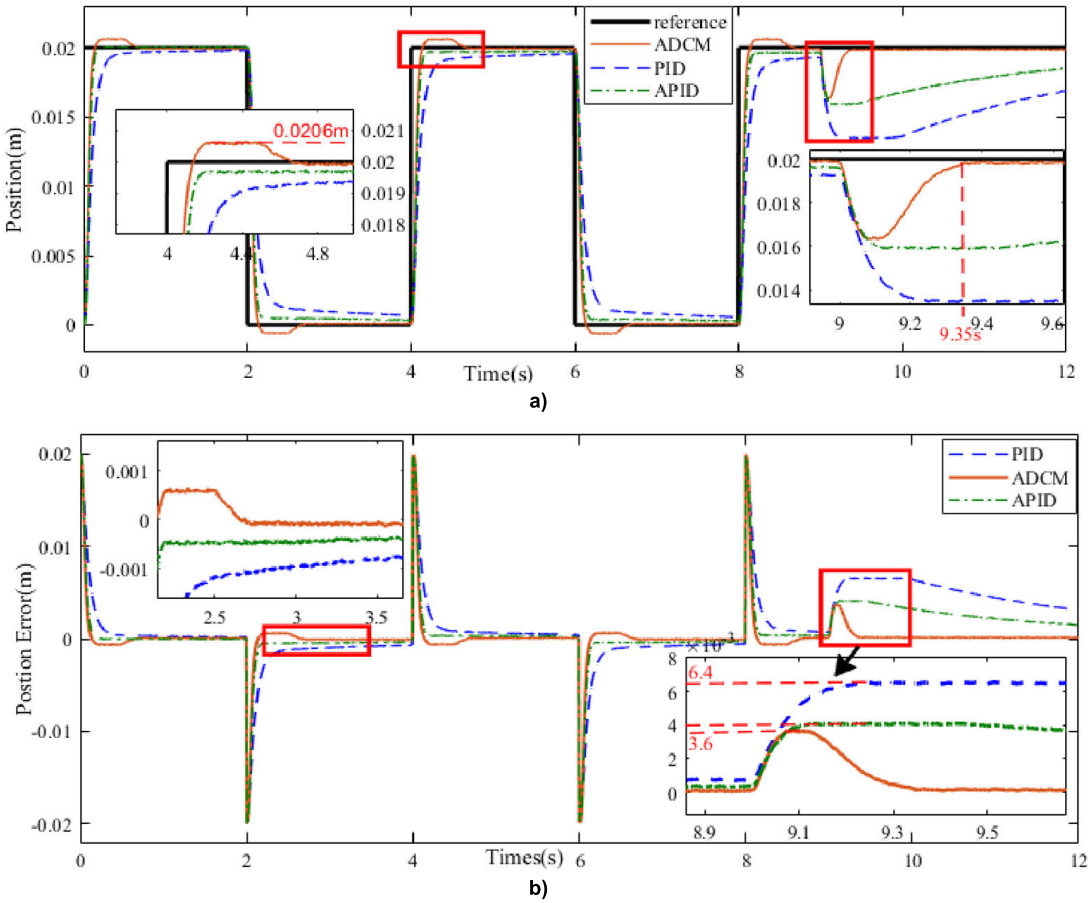

FIGURE 5. Square-wave signal tracking of the EHA model. a) Diagram of the position curves. b) Diagram of the position error.

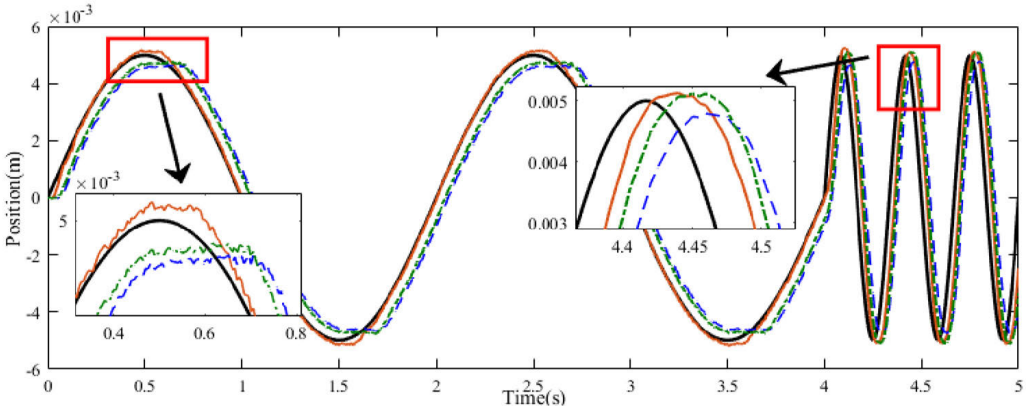

FIGURE 6. Medium to high frequency sinusoidal signal tracking.

nonlinear EDE. Compared with the simulation results obtained for the PID and the APID, the proposed ADCM exhibited better performance in tracking small signals and in defending against the effects of the dead zone.

B. EXPERIMENTAL VALIDATION

An experimental validation based on an EHA test rig was carried out on a platform shown in Fig. 8. Although the experimental setup was well-designed, some factors such as amplitudes of the white noise and the threshold ω_0, were omitted, which made difference to the real applications.

Table 1 summarizes the time span and the averaged velocity when a cylinder moves at a distance of 10mm without external load. The speed of the BLDCM was set as 1.6 revolutions per second (rps) and the deviation was less than 0.1rps. Table.1 shows the time ranged from 94.13s to 225.13s when the theoretical flow rate of the piston pump was almost

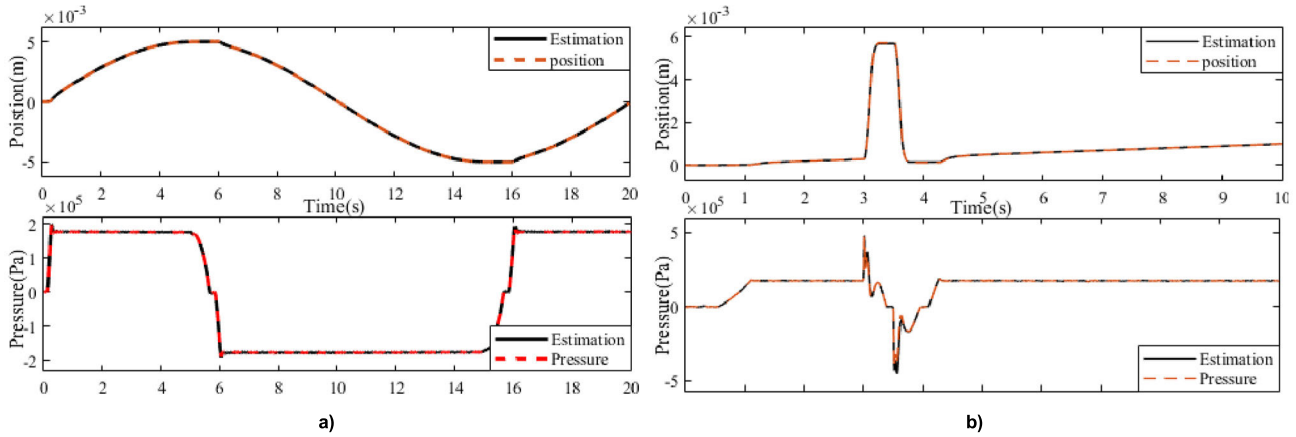

FIGURE 7. State estimations of the EDE of the EHA. a) Sinusoidal reference tracking. b) Ramp reference tracking.

TABLE 1. Experimental results at a constant motor speed combined with no external load condition.

Distance (mm)	Start time (s)	Stop time (s)	Time (s)	Average velocity (mm/s)
30-40	7.21	232.34	225.13	0.044
40-50	3.75	203.8	200.05	0.050
50-60	3.17	97.3	94.13	0.106
60-70	4.74	171.35	166.61	0.060
70-80	3.38	132.8	129.42	0.077

TABLE 2. Main purchased components of the EHA.

Element	Type	Number
Position sensor	FOREVER-CAN-C406	1
Pressure sensor	HM91-AH11V2F1W2	2
Encoder	SG37-2-09.52	1
Mode select valve	HAWE-BVE3ZB2G24-1/2	1

leveled at a constant value. The effects of nonlinear factors caused by the internal leakage of hydraulic components and static friction were illustrated quantitatively because if these factors are small enough to be neglected, then indices of Time and Average Velocity would be bounded in a small range rather than that shown in Table.1.

Table 2 lists the purchased and customized components for establishing the test rig. An internal filter was installed in the position sensor following the manual of the sensors. Pressure signals derived from a second-order Butterworth filter with a 40 Hz cut-off frequency was five times of the referenced bandwidth of the EHA. The related parameters of the latter are shown in Table 3.

The four diagrams in Fig. 9-12 depict the actual displacement response of the EHA. The usage of the digital position sensors effectively attenuated the noises, which was characterized by a smoother evolution of the position curves.

For further comparison in different aspects, the error of steady-state (ESS), overshoot (OS), settling time (ST), amplitude attenuation (AA), phase lag (PL), and robustness (RN) were applied for quantitative illustration.

TABLE 3. Related parameters and the corresponding values of the EHA.

Parameter	Value
Rated pressure	11 MPa
Rated speed	300 mm/s
Rated force	12 kN
Effective movement	0-110 mm
Rated power supply	270 VDC
Bandwidth	5 Hz

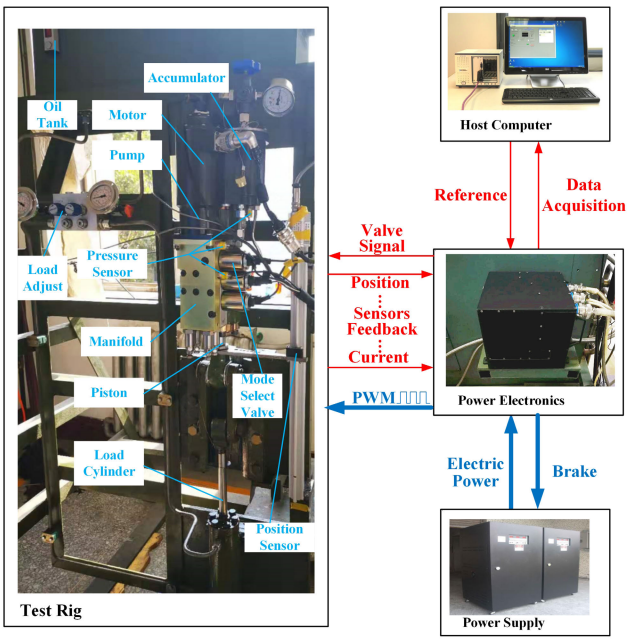

FIGURE 8. EHA prototype test setup.

Robustness was assessed using the absolute maximum error E_m and the mean standard error S_e, which are defined as follows [35]–[37]:

$$E_m = \underset{i=1,\ldots,N}{MAX} |e_i| \tag{27}$$

TABLE 4. Results of experiments.

Specifications		ESS(m)	OS	ST(s)	AA	PL(°)	E_m(m)	S_e(m)
0.05Hz sinusoidal input	PID	-	-	-	4.1%	17.9	10×10^{-4}	18×10^{-6}
	APID	-	-	-	2.8%	10.4	5.3×10^{-4}	9.7×10^{-6}
	ADCM	-	-	-	1.2%	6.1	3.1×10^{-4}	4.9×10^{-6}
3Hz sinusoidal input	PID	-	-	-	12.7%	56.8	38.5×10^{-4}	44.4×10^{-6}
	APID	-	-	-	3.6%	35.4	23.8×10^{-4}	25.2×10^{-6}
	ADCM	-	-	-	0.2%	21.8	16.5×10^{-4}	13.3×10^{-6}
Square-wave signal input	PID	2.4×10^{-4}	1.8%	0.29	-	-	4.34×10^{-4}	258×10^{-6}
	APID	1.2×10^{-4}	2.5%	0.25	-	-	2.67×10^{-4}	157.9×10^{-6}
	ADCM	0.9×10^{-4}	3%	0.19	-	-	1.76×10^{-4}	58.6×10^{-6}
Ramp input (0-3s)	PID	-	-	-	-	-	3.8×10^{-4}	2.7×10^{-6}
	APID	-	-	-	-	-	2.2×10^{-4}	1.4×10^{-6}
	ADCM	-	-	-	-	-	1.2×10^{-4}	0.8×10^{-6}

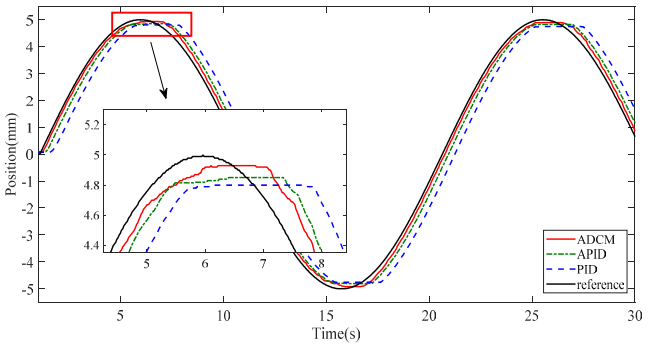

FIGURE 9. Trajectory control with a 0.05 Hz-sine reference.

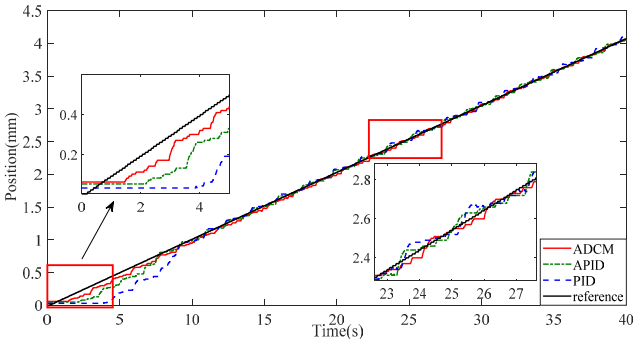

FIGURE 10. Ramp signal tracking with upper and lower boundaries.

$$S_e = \frac{1}{N}\sqrt{\sum_{i=1}^{N}(e_i)^2} \tag{28}$$

The results of the experiments in each aspect were listed in Table.4.

As shown in Fig. 9, the dead zone of the EHA remained its influence on the peak and the trough points of the sine curves. Although some matte phenomenon was observed around these points, the proposed ADCM showed apparent improvements in attenuating the dead-zone effects by comparing with the APID and PID, as indicated in Fig. 3(a). Three criteria out of six, amplitude attenuation, phase lag, E_m and S_e were used to evaluate the dynamic performance of tracking sinusoidal instruction with the frequency ranging from 0.05Hz to 3Hz. 0,05Hz is a pretty low reference for an EHA because the affection of the dead zone will be highlighted, which can be seen in the zoom-in part in Fig. 9. However, in ADCM, the effort of integral action supposed to hedge against the dead zone was replaced by the compensation from P-EDE and C-EDE. Thus, the index E_m (with ADCM) is 3.1×10^{-4} that is much smaller than both APID and PID. Simultaneously, little AA and PL were found. Noting that the output of PID and APID fully hinges on position error such that error of position and PL are inevitable. Two equations, (17) and (21), told that outcome of ADCM consists of estimated part and error part hence the decrease of amplitude attenuation and

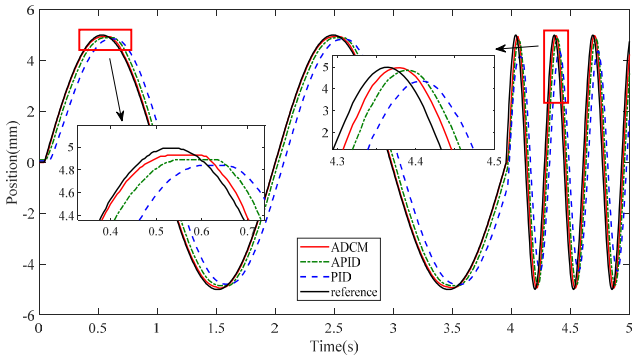

FIGURE 11. Sinusoidal input performance at medium to high frequency.

phase lag is reasonable. Accordingly, a reduction of 4.3° was found by comparing ADCM and APID. Further, as the frequency of reference rose to 3Hz in Fig. 11, the developed ADCM still led the best dynamic characteristic with a phase lag of 21.8° and the attenuation that was barely observed.

The output of the low-velocity experiments in Fig. 10 indicated that the proposed method was able to precisely track the reference signals since the response curves coincided with the expected displacement except for the initial 2s. According to the zoomed part, the initial points were located at around 0 mm, which was resulted from

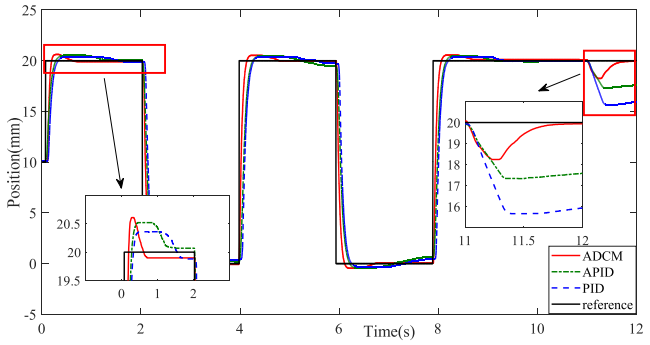

FIGURE 12. Square-wave input response of the EHA with an external load.

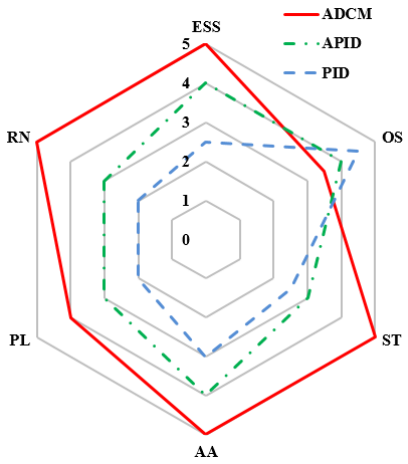

FIGURE 13. Radar map of experimental results.

the minimum resolution of the position sensor is 0.01 mm. Furthermore, the second zoomed view also indicates the superiority of ADCM over tracking a tiny expected displacement since comparing with APID and PID, the red line seldom overpass the desired position. In ramp-signal tests, E_m and S_e were adopted to analyze tracking accuracy and chattering around the reference. The maximum position error of ADCM is 1.2×10^{-4} which get a 46% and 69% decrease by comparing with APID and PID, respectively. Consequently, the proposed ADCM demonstrates an advantage in robustness by estimating parameters uncertainties of the EHA.

The square-wave response of the EHA is illustrated in Fig. 12. Combined with the results shown in Fig. 5(a), the comparison of square-wave trajectory at an amplitude of 20mm and a frequency of 0.25Hz can be observed. Although a tiny deviation could still be observed, the overall evolution trend of the displacement obtained from simulation showed a high consistency to that gathered from experiments, except that overshoot occurred with PID and APID controllers, which resulted from the combined mass of the connecting block and load cylinder. Table 4 shows that the overshoot of the developed method is 3%, which is acceptable, despite being slightly larger than APID. Nevertheless, experimental results still confirmed the effectiveness of the improvements of the ADCM on the rapidness and accuracy. Additionally, an external workload disturbance with an amplitude of 1800N generated by the load cylinder was applied on the EHA at around 11s and then we calculated E_m and S_e, and stopped counting ESS, OS, and ST at the same time. As depicted by the zoomed part in Fig. 11 and Table 4, only a 1.76mm degradation of position occurred due to the resistance against the external load force and the process of recovery was completed within 0.5 seconds with compensation from the designed estimators. However, because tuning controller gains online, the compensation speed was dilatory for an EHA despite the effort of integral of APID being much faster than PID. Therefore, by observing the index square-wave signal input, E_m and S_e demonstrated that the proposed ADCM exhibited higher performance as compared to traditional control methods, e.g. PID and APID, in the resistance to parametric uncertainties and unknown workload.

Pursuing a visualized comparison among the controllers, Fig. 13 illustrates three algorithms in the six aspects. For an EHA, the importance of the six aspects varies along with the specific application. Hence, in this research, we defined them to be equally significant. Compared with the APID and the PID, the proposed ADCM achieved higher ESS, PL, AA and the most importantly, RN abilities, which are beneficial mainly for the estimation and compensation of the internal and external disturbance of the implemented EDE. An overshoot occurs as the EHA system tracks a big step signal and as a result, the ADCM was a little less competitive in terms of the overshoot region because the settling time would be extended accordingly when the EHA system tracks a big step signal, which is suitable for the APID because of its large step-input situation. Generally, the proposed ADCM had the best performance compared with the two selected traditional control solutions.

V. CONCLUSION

In this paper, a nonlinear model of an EHA was established, and a four-loop cascade control was proposed based on ADCM to enhance the ability of the EHA, particularly in the low-velocity zone where the nonlinear and the uncertainties significantly impair the performance of EHA. The results of simulations showed the designed control strategy had strong stability and robustness to overcome the uncertainties and other nonlinear factors of the EHA. Based on the results of experiments, the EDE, an essential component of the ADCM, is proven to be a powerful tool for estimating the external disturbance and compensate for system uncertainties in hydraulic and mechanical subsystems. Robustness, rapidness, and accuracy of the ADCM controller were also validated through the test rig and simulation. Some parametric optimization is still required to improve the performance of the proposed EHA system further, which will be conducted in the next work.

NOMENCLATURE

Sybmol	comment	unit
x	Cylinder displacement	m
u	Bus voltage	270V
i	Bus current	A
e_a,e_b,e_c	Back electro-motive force (EMF)	V
L	Line induction of the motor	1.33mH
R	Line resistant of the motor	0.2Ω
T_e	Electromagnetic torque	N
K_t	Electromagnetic torque coefficient	N·m/A
J_{mp}	Total inertia	4×10^{-4}kg·m^2
B_m	Total vicious friction coefficient	6×10^{-4}N·m/(rad/s)
T_L	External load	N·m
ω	Rotary speed of the motor	rad/s
D_p	Pump displacement,	0.398cm^3/rad
$p_{a,b}$	Pressures of two chambers of the piston pump	Pa
p_r	System back pressure	Pa
β_e	Effective oil bulk modulus	6.86×10^8N/m^2
Q_aQ_b	Inlet and outlet flow rates of the piston pump	L/min
Q_1Q_2	Supplied and returned flow rates of the cylinder	L/min
Q_f	Unconsidered leakage	L/min
A	Effective ram area of the cylinder	1.13×10^{-3}m^2
V_aV_b	Initial volume of each chamber	4×10^{-4}m^3, 4×10^{-4} m^3
L_2	Internal leakage coefficient of the cylinder	5×10^{-11} (m^3/s)/Pa
V_0	Mean volume of the system including chambers and pipes	4×10^{-4} m^3
B_c	Viscous friction coefficient of the cylinder	760N/(m/s)
K_s	The elastic load	N/m
F_f	Unmodeled friction	N
F_L	External load force	N
$x_i(i=1,2\ldots5)$	System state vectors	
$a_i(i=1,2,3)$	Nonlinear friction coefficients	2.1. $\times10^4$, -1450, 46
h_p, h_c	Extended equivalent disturbances	
n_p	Measured noise	
δ, α	Tunable parameters of the estimator	
k_{pp},k_{pd}	Proportionality and differential coefficients of the position loop	
k_{pc}	Proportionality of tge compression loop	
$l_{pi}(i=1,2,3)$	Estimator gain of the position loop	
$l_{ci}(i=1,2)$	Estimator gain of the compression loop	

ACKNOWLEDGMENT

The authors would like to thank the anonymous reviewers who provided valuable comments and suggestions.

REFERENCES

[1] T. Yu, A. R. Plummer, P. Iravani, J. Bhatti, S. Zahedi, and D. Moser, "The design, control, and testing of an integrated electrohydrostatic powered ankle prosthesis," *IEEE/ASME Trans. Mechatronics*, vol. 24, no. 3, pp. 1011–1022, Jun. 2019.

[2] W. Wu and C. Yu, "Simulation and experimental analysis of hydraulic directional control for displacement controlled system," *IEEE Access*, vol. 6, pp. 27993–28000, 2018.

[3] B. Yu and W. Shu, "A novel control approach for a thrust vector system with an electromechanical actuator," *IEEE Access*, vol. 5, pp. 15542–15550, 2017.

[4] A. Navatha, K. Bellad, S. S. Hiremath, and S. Karunanidhi, "Dynamic analysis of electro hydrostatic actuation system," *Procedia Technol.*, vol. 25, pp. 1289–1296, Jan. 2016.

[5] J. Kovar, "Electro-hydraulic control of injection moulding machine for plastic," *Rev. Sci. Instrum.*, vol. 65, no. 11, pp. 3408–3414, 2011.

[6] J. Zhao *et al.*, "Review of the cylinder block/valve plate interface in axial piston pumps: Theoretical models, experimental investigations, and optimal design," *Chin. J. Aeronaut.*, vol. 43, no. 2, pp. 1–20, 2021.

[7] J. Yao, G. Yang, and D. Ma, "Internal leakage fault detection and tolerant control of single-rod hydraulic actuators," *Math. Problems Eng.*, vol. 2014, pp. 1–14, Mar. 2014, Art. no. 345345.

[8] G. Ren, M. Esfandiari, J. Song, and N. Sepehri, "Position control of an electrohydrostatic actuator with tolerance to internal leakage," *IEEE Trans. Control Syst. Technol.*, vol. 24, no. 6, pp. 2224–2232, Nov. 2016.

[9] L. Jun, F. Yongling, W. Zhanlin, and Z. Guiying, "Research on fast response and high accuracy control of an airborne electro hydrostatic actuation system," in *Proc. Int. Conf. Intell. Mechatronics Autom.*, Chengdu, China, 2004, pp. 428–432.

[10] J.-M. Zheng, S.-D. Zhao, and S.-G. Wei, "Application of self-tuning fuzzy PID controller for a SRM direct drive volume control hydraulic press," *Control Eng. Pract.*, vol. 17, no. 12, pp. 1398–1404, Dec. 2009.

[11] D. M. Wonohadidjojo, G. Kothapalli, and M. Y. Hassan, "Position control of electro-hydraulic actuator system using fuzzy logic controller optimized by particle swarm optimization," *Int. J. Autom. Comput.*, vol. 10, no. 3, pp. 181–193, Jun. 2013.

[12] Y. Jia, "Robust control with decoupling performance for steering and traction of 4WS vehicles under velocity-varying motion," *IEEE Trans. Control Syst. Technol.*, vol. 8, no. 3, pp. 554–569, May 2000.
[13] Y. Jia, "Alternative proofs for improved lmi representations for the analysis and the design of continuous-time systems with polytopic type uncertainty: A predictive approach," *IEEE Trans. Autom. Control*, vol. 48, no. 8, pp. 1413–1416, Aug. 2003.
[14] L. Yang, S. Yang, and R. Burton, "Modeling and robust discrete-time sliding-mode control design for a fluid power electrohydraulic actuator (EHA) system," *IEEE/ASME Trans. Mechatronics*, vol. 18, no. 1, pp. 1–10, Jul. 2011.
[15] Y. C. Zhang and X. Y. Qi, "Study of electro-hydraulic actuator based on PID and sliding mode control," *Mach. Tool Hydraul.*, vol. 45, no. 21, pp. 122–126, 2017.
[16] C. C. Soon, R. Ghazali, H. I. Jaafar, and S. Y. S. Hussien, "Sliding mode controller design with optimized PID sliding surface using particle swarm algorithm," *Procedia Comput. Sci.*, vol. 105, pp. 235–239, Jan. 2017.
[17] S. Wang, S. Habibi, and R. Burton, "Sliding mode control for an electro-hydraulic actuator system with discontinuous non-linear friction," *Proc. Inst. Mech. Eng., I, J. Syst. Control Eng.*, vol. 222, no. 8, pp. 799–815, Dec. 2008.
[18] R. Yang, Y. Fu, L. Zhang, H. Qi, X. Han, and J. Fu, "A novel sliding mode control framework for electrohydrostatic position actuation system," *Math. Problems Eng.*, vol. 2018, Jan. 2018, Art. no. 7159891.
[19] J. M. Lee, S. H. Park, and J. S. Kim, "Design and experimental evaluation of a robust position controller for an electrohydrostatic actuator using adaptive antiwindup sliding mode scheme," *Sci. World J.*, vol. 2013, pp. 1–16, Jan. 2013, Art. no. 590708.
[20] A. Ayadi, S. Hajji, M. Smaoui, A. Chaari, and M. Farza, "Experimental sensorless control for electropneumatic system based on high gain observer and adaptive sliding mode control," *Int. J. Adv. Manuf. Technol.*, vol. 93, nos. 9–12, pp. 4075–4088, Dec. 2017.
[21] J. F. Carneiro and F. G. de Almeida, "Accurate motion control of a servopneumatic system using integral sliding mode control," *Int. J. Adv. Manuf. Technol.*, vol. 77, nos. 9–12, pp. 1533–1548, Apr. 2015.
[22] H. Zhang, X. Liu, J. Wang, and H. R. Karimi, "Robust H_∞ sliding mode control with pole placement for a fluid power electrohydraulic actuator (EHA) system," *Int. J. Adv. Manuf. Technol.*, vol. 73, pp. 1095–1104, Jul. 2014.
[23] W. Sun, H. Gao, and B. Yao, "Adaptive robust vibration control of full-car active suspensions with electrohydraulic actuators," *IEEE Trans. Control Syst. Technol.*, vol. 21, no. 6, pp. 2417–2422, Nov. 2013.
[24] X. Song, Y. Wang, and Z. Sun, "Robust stabilizer design for linear time-varying internal model based output regulation and its application to an electrohydraulic system," *Automatica*, vol. 50, no. 4, pp. 1128–1134, Apr. 2014.
[25] Q. Guo, J. Yin, T. Yu, and D. Jiang, "Saturated adaptive control of an electrohydraulic actuator with parametric uncertainty and load disturbance," *IEEE Trans. Ind. Electron.*, vol. 64, no. 10, pp. 7930–7941, Oct. 2017.
[26] H. Sun, T. Meinlschmidt, and H. Aschemann, "Passivity-based control of a hydrostatic transmission with unknown disturbances," in *Proc. 19th Int. Conf. Methods Models Autom. Robot. (MMAR)*, Miedzyzdroje, Poland, Sep. 2014, pp. 94–99.
[27] K. K. Ahn, D. N. C. Nam, and M. Jin, "Adaptive backstepping control of an electrohydraulic actuator," *IEEE/ASME Trans. Mechatronics*, vol. 19, no. 3, pp. 987–995, Jun. 2014.
[28] S. Sakaino and T. Tsuji, "Oil leakage and friction compensation for electro-hydrostatic actuator using drive-side and load-side encoders," in *Proc. 42nd Annu. Conf. IEEE Ind. Electron. Soc. (IECON)*, Florence, Italy, Oct. 2016, pp. 5088–5093.
[29] J. Yao, Z. Jiao, and S. Han, "Friction compensation for low velocity control of hydraulic flight motion simulator: A simple adaptive robust approach," *Chin. J. Aeronaut.*, vol. 26, no. 3, pp. 814–822, Jun. 2013.
[30] C. Wang, L. Quan, Z. Jiao, and S. Zhang, "Nonlinear adaptive control of hydraulic system with observing and compensating mismatching uncertainties," *IEEE Trans. Control Syst. Technol.*, vol. 26, no. 3, pp. 927–938, May 2018.
[31] X. Wang, C. Shi, and S. Wang, "Extended state observer-based motion synchronisation control for hybrid actuation system of large civil aircraft," *Int. J. Syst. Sci.*, vol. 48, no. 10, pp. 2212–2222, Jul. 2017.
[32] H.-J. Wang, K. Zhu, G.-I. Shi, M. Tanida, M. Hayashi, and M. Shinagawa, "Performance of swash-plate type axial piston pump with different rotation rates," *Hydraulic Pneum.*, vol. 8, no. 8, pp. 100–106, 2017.
[33] B.-Z. Guo and Z.-L. Zhao, "On the convergence of an extended state observer for nonlinear systems with uncertainty," *Syst. Control Lett.*, vol. 60, no. 6, pp. 420–430, Jun. 2011.
[34] B.-Z. Guo and Z.-L. Zhao, "On convergence of the nonlinear active disturbance rejection control for MIMO systems," *SIAM J. Control Optim.*, vol. 51, no. 2, pp. 1727–1757, Jan. 2013.
[35] A. Bonchis, P. I. Corke, and D. C. Rye, "Experimental evaluation of position control methods for hydraulic systems," *IEEE Trans. Control Syst. Technol.*, vol. 10, no. 6, pp. 876–882, Nov. 2002.
[36] M. Choux and G. Hovland, "Adaptive beckstepping control of nonlinear hydrauic-mechanical system including valve dynamic," *Model., Identificat. Control*, vol. 31, no. 1, pp. 35–44, 2010.
[37] R. Ghazali, Y. M. Sam, M. F. Rahmat, C. C. Soon, H. I. Jaafar, and Z. Has, "Discrete sliding mode control for a non-minimum phase electro-hydraulic actuator system," in *Proc. 10th Asian Control Conf. (ASCC)*, May 2015, pp. 1–6.
[38] F. J. Goforth and Z. Gao, "An active disturbance rejection control solution for hysteresis compensation," in *Proc. Amer. Control Conf.*, Washington, DC, USA, Jun. 2008, pp. 2202–2207.

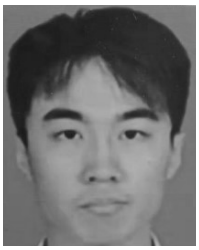

MINGKANG WANG (Student Member, IEEE) received the B.S. degree from the School of Mechanical Engineering and Automation, Beijing University of Chemical Technology, China, in 2015. He is currently pursuing the Ph.D. degree with the School of Mechanical Engineering and Automation, Beihang University, China. His research interests include hydraulic servomechanism, servo control of mechatronic systems, and disturbance active compensation control theory.

YAN WANG is currently an Associate Professor with Beihang University, China. His main research interests include servo control of electro-hydraulic systems, numerical simulation and control of fluid transmission, and so on.

YONGLING FU received the M.S. and Ph.D. degrees in fluid power transmission and control from the Harbin Institute of Technology, China. He is currently a Professor with the School of Mechanical Engineering and Automation, Beihang University. His research interests include advanced aircraft hydraulic systems, power telex integration servo operating systems, electromechanical fluid control integrated systems, and special industrial robots.

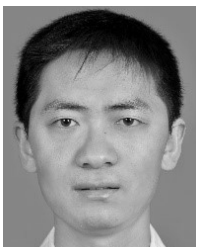

RONGRONG YANG received the B.S. and M.S. degrees in control theory and control engineering from the Lanzhou University of Technology, Lanzhou, China, in 2002 and 2007, respectively, and the Ph.D. degree in mechatronic engineering from Beihang University, Beijing, China, in 2019. He is currently a Lecturer with the School of Mechanical and Electrical Engineering, Lanzhou University of Technology. His current research interests include servo control of electromechanical and electro hydraulic systems, robust adaptive control, and disturbance active compensation control.

JIANG'AO ZHAO received the B.S. degree from the School of Mechanical Engineering, Yanshan University, China, in 2013. He is currently pursuing the Ph.D. degree with the School of Mechanical Engineering and Automation, Beihang University. His research interests include high-speed high pressure piston pump and hydraulic servo systems.

JIAN FU (Member, IEEE) received the B.S. degree in electronic information and control engineering from the Beijing University of Technology, in 2008, and the double Ph.D. degrees from INSA-Toulouse and Beihang University, in 2017. He is currently an Assistant Professor with the School of Mechanical Engineering and Automation, Beihang University. His research interests include intelligent manufacturing systems and actuation system design and control.